2008 American Control Conference
Westin Seattle Hotel, Seattle, Washington, USA
June 11-13, 2008

High-Speed Serial-Kinematic AFM Scanner: Design and Drive Considerations

Kam K. Leang†
Department of Mechanical Engineering
Virginia Commonwealth University
Richmond, Virginia, 23284-3015, USA

Andrew J. Fleming‡
School of Electrical Eng. and Computer Science
The University of Newcastle
Callaghan, NSW 2308, Australia

Abstract— **In this paper, we describe the design of a flexure guided, two-axis nanopositioner driven by piezoelectric stack actuators. The scanner is specifically designed for high-speed scanning probe microscope (SPM) applications. A high-speed atomic force microscope (AFM) is required to acquire high resolution, three-dimensional, time-lapse images of fast processes such as the rapid movement of cells and the diffusion of DNA molecules. High-speed scanner designs have been proposed, for example, by Ando and co-workers as well as Schitter and co-workers, for AFM imaging. In the proposed design, the slow and fast scanning axes are serially connected and both axes are flexure-guided to minimize runout. The achievable scan range is 10 $\times$ 10 μm. The scanner's mechanical resonance frequencies were optimized using finite element analysis. Experimental results show a first major resonance, in the slow and fast axis respectively, at approximately 1.5 kHz and 29 kHz. In addition to evaluating the proposed design, this paper also discusses the various tradeoffs between speed, range, and required control hardware. Electrical requirements and scan trajectory design are also considered.**

I. Introduction

The dynamic behavior of biological cells, DNA, and molecules occur at time scales much faster than the measurement capabilities of conventional scanning probe microscopes (SPM's), for example, an atomic force microscope (AFM). High-speed AFM is required to observe these processes in real-time [1]. Also, high-speed positioning is desired to enable high-throughput probe-based nanomanufacturing. Being primarily a serial technique, the total process time of probe-based fabrication is proportional to the number of desired features [2]. A higher speed positioning stage greatly improves the throughput of such manufacturing processes. We propose a serial-kinematic scanner where the lateral (x) axis is designed for high-speed scanning and the transverse (y) axis is for low-speed scanning.

Several high-speed scanning stages have been proposed. For example, earlier work by Ando and co-workers [3] focused on exploiting stiff piezo-stack actuators to create a scanner with high resonance frequency. The researchers demonstrated imaging at 12.5 frames/s (100 $\times$ 100 pixels per image), and they used the system to capture real-time video of biological specimens [4]. Schitter and co-workers also developed a scanner based on piezo-stack actuators, but these were arranged in a push-pull configuration with mechanical flexures to decouple the lateral and transverse axes [5]. The finite element analysis (FEA) method was used to optimize the performance of the mechanical structure [6]. The reported AFM imaging rate was 8 frames/s (256 $\times$ 256 pixels). By exploiting the stiffness of shear piezos and a compact design, a scanner was created for imaging up to 200 frames/s (256 $\times$ 32 pixels) [7]. The achievable range of motion in the proposed design was 300×300 nm^2. A unique approach was presented for high speed scanning in which a piezo-stack actuator was combined with a tuning fork. The tuning fork operated at resonance [8] and AFM images were acquired at 100 frames/s (128 $\times$ 128 pixels).

In this paper, a serial-kinematic scanner design is proposed. The tradeoffs between speed, range, required control hardware, cost and manufacturability are considered. In the next section, design objectives are discussed. Following that, details of the mechanical design are presented in Section III. Sections V and IV discuss the design of input trajectories and the electrical requirements of the driving amplifier. Preliminary experimental results are then presented in Section VI followed by conclusions in Section VII.

II. Design Objectives and Considerations

The goal is to develop a high-speed scanner to move a sample relative to an SPM, such as AFM, probe tip. To achieve this goal, we considered the following features. First, the frame rate should be at least 30 frames per second, where each frame is 100 $\times$ 100 pixels. Second, the desired scan range was $\geq 10 \times 10$ μm^2. The required range enables the AFM to observe a wide spectrum of specimens and samples, from micron-size cells to submicron size subjects such as DNA. Finally, we wanted the system to be cost effective to manufacture.

The design process included: (1) identifying relevant design tradeoffs, (2) optimizing the mechanical design of the scanner using FEA, (3) developing the necessary electronic hardware for the scanner, and (4) considering the use of input-shaping to enable high-speed scanning. We focused the attention on the motion parallel to the sample surface, *i.e.*, along the lateral (x) and transverse (y) directions. Future work will deal with movements in the vertical (z) axis.

The following design parameters were deemed important: (i) the first dominant resonant frequency, (ii) the scanning range, (iii) the power supply requirements (voltage, current, and bandwidth), and (iv) the cost and manufacturability. This work focused on mechanical design of the scanner, and we

†kkleang@vcu.edu, Voice/Fax: +1.804.827.7037/7070.
‡Andrew.Fleming@newcastle.edu.au, Voice: +61.2.4921.6493.

did not factor in the details of the required control system hardware. These issues will be addressed at a later time.

The first two design parameters, (i) and (ii), conflict directly with one another. Large range implies low stiffness and hence low first resonance frequencies [6].

The third design parameter restricts the amount of voltage, current, and power that can be supplied to the actuator. This, in turn, restricts the type and dimensions of the piezoactuator that can be used. Larger piezoelectric actuators can provide greater stroke, but have higher capacitance and require more power at high frequencies to drive. The final consideration is cost and manufacturability. The scanner fabrication should not utilize any exotic materials or processes and should be tolerant of acceptable machining tolerances. These considerations are discussed in the following sections with more detail.

III. The Mechanical Design

A. Serial Versus Parallel Kinematic Configuration

For scanning in two directions, there are two basic configurations: serial and parallel kinematics. In a serial kinematic system, for example the design used by several commercial vendors of scanning stages and in [4], there is exactly one actuator (and sensor) for each degree of freedom [see Fig. 1(a)]. One disadvantage of this design is the inability to measure (and correct for) parasitic motion such as runout or guiding error. Although the serial configuration is simple to design, a penalty is that high resonance frequency can only be achieved in one axis.

In a parallel kinematic scanning stage (*e.g.*, Schitter *et al.*'s work [9]), all actuators are connected in parallel to the sample platform [see Fig. 1(b)]. This arrangement enables rotation of the image, *i.e.*, the fast scanning axis can be chosen arbitrarily. An advantage of this configuration is the parasitic motion due to runout and guiding error can easily be measured and corrected. However, since the mechanical dynamics of both the lateral and transverse axes are similar, high-bandwidth control hardware is needed for both directions. This added inconvenience can increase the overall cost of the system.

In both configurations, the spring constants k_x and k_y may include the stiffness of added flexures in each direction (see Fig. 1). To achieve high resonance frequencies, the effective spring constants should be as stiff as possible while maintaining low effective mass. The effect of inertial force generated by the sample platform must also be taken into account. The flexures must provide enough preload to avoid exposing the stack actuator to damaging tensional forces.

In this work, a serial-kinematic configuration is explored [see Fig. 1(a)]. One axis, the x axis, is for fast scanning. The other axis, the y axis, is for slow-speed scanning. Therefore, only one axis requires high power and wide bandwidth performance. The overall cost of driver electronics is reduced by essentially half.

While the resonance frequency of the fast axis is of primary concern, the slow axis resonance frequency can essentially be ignored. This is due to its slow speed of operation, for example, one-hundredth the fast axis scan rate when acquiring a 100×100 pixel image. This allows the fast scan axis to be designed independently without any significant consideration for performance implications on the slow-scan axis.

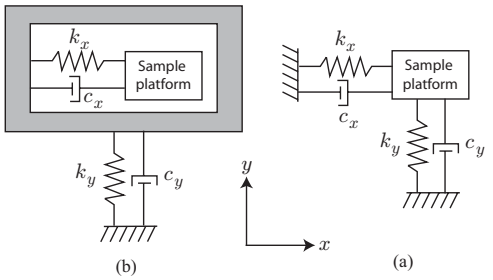

Fig. 1. Configurations for two-axis scanning: (a) serial and (b) parallel kinematics arrangement. The spring constants k_x and k_y include the stiffness of the piezoactuators and added flexures in each direction.

TABLE I
A comparison of different piezoactuator types.

Actuator type	Stiffness	Range	Capacitance	Voltage
Piezo-bimorph	low	high	med	low-med
Piezo-tube	med	med	low	high
Piezo-plate	high	low	low	high
Piezo-stack	high	low-med	med-high	low

B. Piezoactuator Considerations

The actuating mechanism of choice for scanning at high speed is the piezoactuator [10]. We compared different types of piezoactuators, see Table I. There are many available geometries, for example, tube-shaped (piezo-tube), shear piezo, piezo-bimorph, and piezo-stack actuators. Piezo-stack actuators offer high stiffness, but limited range of motion. The geometry of a stack compared to a tube-shaped piezoactuator results in higher resonance frequencies for the same deflection [11]. Thin shear-piezos offer high resonance frequency, but small range (sub-micron) [7].

For the desired scan range of 10×10 μm, the Noliac SCMA-P7 piezoelectric stack actuators were chosen (5 mm$\times$ 5 mm $\times$ 10 mm, 380 nF). The actuator stroke is 11.8 μm, with an unloaded resonance frequency of 220 kHz, stiffness of 283 N/μm, and blocking force of 1000 N. The elastic modulus calculated from the blocking pressure P_B and strain ϵ is $E = \frac{P_B}{\epsilon} = 33$ GPa.

The capacitance of the piezoactuator was also considered. Although a greater cross-sectional area would increase stiffness, the proportional increase in capacitance and required power is highly undesirable.

C. Preloading Piezo-Stack Actuators

Piezo-stacks are intolerant to tensile (as well as shear) stresses. Because stacks are made by gluing (or fusing) together individual layers of piezoelectric material, tension loads can cause the actuators to fail at the interface (glue) layers. Manufacturers often report that tensile forces must not

TABLE II

THE MECHANICAL PROPERTIES OF VARIOUS METALS [12].

Metal	Elastic modulus (GPa)	Yield strength (MPa)	Density (kg/cm^3)	Poisson's Ratio
Aluminum alloy	72	97	2800	0.33
Stainless steel	200	207	8000	0.30
Titanium	107	240	4510	0.36

exceed 5 to 10% of the compressive load limit. During high speed scanning, the inertia forces (for example due to the sample mass) must be taken into account to avoid excessive tensile stresses. A preload force must be incorporated into the motion mechanism to compensate for the inertial load. Also, the preload must be applied in such a way that full surface contact (no point contact) is achieved to assure good load distribution.

In our design, we propose the use of flexures to apply the appropriate preload on the piezo-stack actuator. The flexures serve two purposes: to eliminate tensile stress and to guide the extension/contraction of the actuator so that parasitic motion is minimized. The required preload was estimated from Newton's law by computing the maximum sample platform acceleration during maximum excursion and scan frequency. In Section IV an input signal is designed that minimizes induced vibration. For this trajectory, the minimum preload requirement is 20 N for a 2 g sample mass. With a safety factor of 2, the conservative preload specification is 40 N. The flexure design which provides this preload force is discussed next.

D. Optimizing the Mechanical Design using FEA

The finite element method (ANSYS, Canonsburg, PA 15317, USA) was used to optimize the design of the scanner in both directions [6]. Since we opted for the serial-kinematic configuration, the first task was to design the high-speed scanning stage (x-axis). Various metals were considered for the design as listed in Table II [12]. We chose stainless steel and AISI A2 tool steel for the stage body because of their high stiffness compared to the piezoelectric material. We note that the AISA A2 steel requires proper heat treating to achieve the equivalent elastic modulus as stainless steel. Other components, such as the flexures and sample platform, where a high stiffness to density ratio was desired, were made from aluminum.

For the high-speed axis, the piezo-stack was fixed on one side, and the sample platform (plate) was attached to the free end. Preloading is achieved by using two flexures attached to the free end, connected to the sample platform, as shown in Fig. 2. Also shown in the figure is an opposing piezo-stack, which was added to compensate for inertial force generated by the movement of the sample platform. These inertial forces can induce undesirable dynamics on both the low- and high-speed stages.

The preload on the piezo-stack was achieved when the stage was assembled. In particular, the preload was achieved by "squeezing" the stack into the flexures using fasteners.

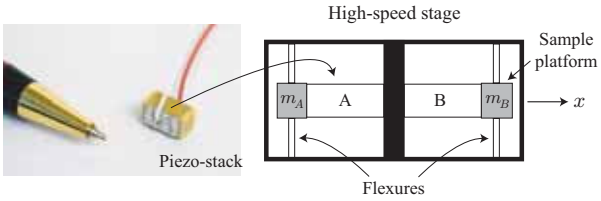

Fig. 2. (Left) A photograph of the piezo-stack actuator and (Right) a sketch of the flexure-guided high-speed stage, where an opposing piezo-stack is used to compensate for the sample platform's inertial effects. These effects can induce unwanted movement on the low-speed (y-axis) stage.

The dimensions of the flexures were designed to provide the appropriate preload when the stage was assembled. The flexures helped to shift the first resonance frequency of the piezo-stack to a higher value compared to the cantilevered configuration. We designed the flexure by assuming linear-elastic behavior of the material and using beam analysis. In the configuration shown in Fig. 2, we modelled the flexures as a fixed-fixed (clamp-clamp) beam with a point load P at the center. The maximum deflection for such a beam occurs at its midpoint [13], for example, where the sample platform makes contact with the flexure,

$$\delta_{max} = \frac{PL^3}{192EI}, \tag{1}$$

In Eq. (1), E is the elastic modulus, L is the length (*i.e.*, combined length of both vertical flexures), and $I = ht^3/12$ (t and h are the thickness and height of the flexure). Rewriting the deflection equation (1), the flexure's spring constant is

$$K_f = \frac{192EI}{L^3}, \tag{2}$$

and this expression was used to determine the required dimensions of the flexure given the stiffness K_f. We chose the flexure stiffness $K_f = 10$ N/μm, roughly $1/20^{th}$ the stiffness of the piezo-stack. Likewise, the low-speed stage was designed in a similar manner.

Due to manufacturing tolerances [± 0.001 in (± 25 μm)], the preload exerted by the flexure on the piezo-stack can be as high as 250 N. This value, though greater than the estimated value of 40 N, is acceptable. An assembly drawing and a photograph of the two-axis high-speed scanner is shown in Fig. 3(a) and (b), respectively.

ANSYS FEA software was used to simulate the dynamics of the low- and high-speed stage. The simulated frequency response from applied voltage to the normalized displacement are plotted in Fig. 4. The three plots (top-to-bottom) show the magnitude response of the x-, y- and z-axis, respectively. The edges of the flexures and the base of the piezo-stack were constrained in the FEA simulation; that is, we neglected the body modes.

The simulation results in Fig. 4 indicate that the lowest resonance occurs at approximately 28.5 kHz (the vertical cantilever mode of the piezo-stack). The next dominant mode is the side-to-side (y-axis) motion, which presents itself at 33 kHz. Finally, the piston mode of the piezo-stack (in the

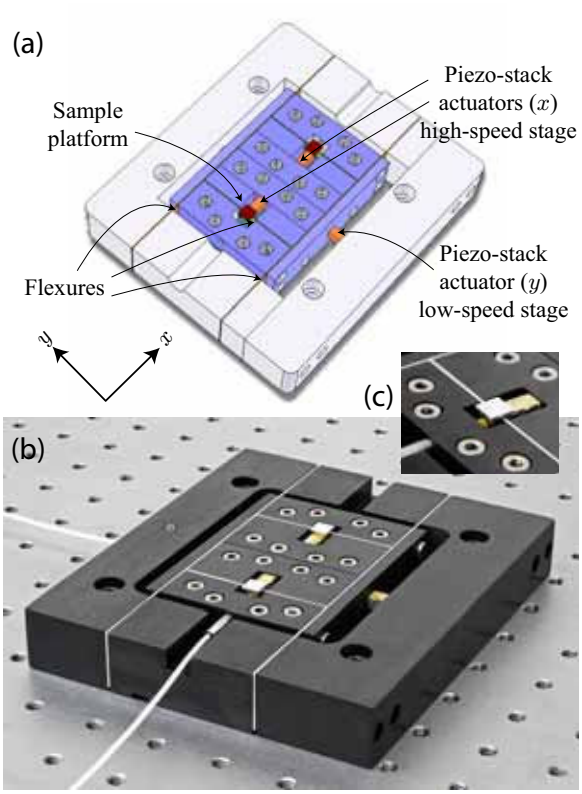

Fig. 3. (a) An assembly drawing of the two-axis high-speed scanner, where the high-speed stage (x) is nested inside of the low-speed stage (y). (b) A photograph of a manufactured scanner with black surface finish. (c) A close-up view of sample platform and x-axis piezo-stack actuator.

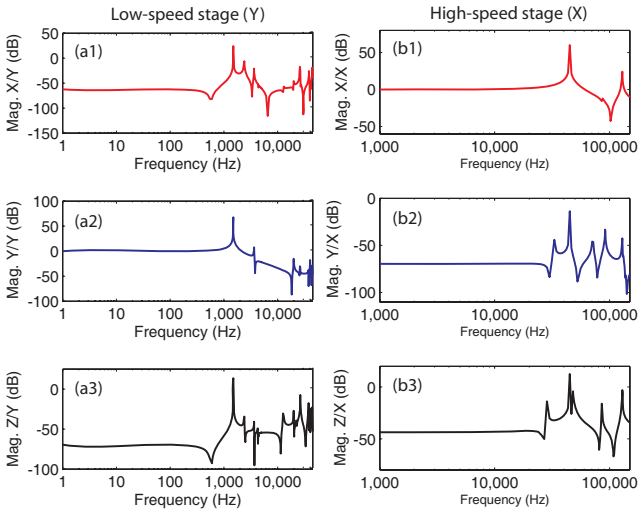

Fig. 4. Simulated frequency response for the low-speed (y-axis) stage, plots (a1) to (a3), and for the high-speed (x-axis) stage, plots (b1) to (b3).

x-axis) occurs at 45 kHz. Along the low-speed axis, the dominant mode occurred at approximately 1.5 kHz. We note that the resonance frequency for the low-speed stage can be improved by reducing the mass of the high-speed stage.

IV. Input Design

The characteristics of the input signal determines the maximum scan rate, induced vibration, minimum mechanical preload, and electrical requirements of the drive electronics. Therefore, the input signal significantly influences the overall scanner performance and should be optimized accordingly.

In high-speed applications, the primary goal is to achieve the highest possible scan-rate from a given mechanical bandwidth. Various inversion-based feedforward controllers have been proposed with this aim, for example [14], [15]. Unfortunately, such techniques require detailed plant models and can not guarantee linear scanning (constant velocity) operation.

Recently a technique was introduced to design periodic input signals with perfectly linear regions and optimal spectral characteristics [16]. The resulting signals minimize signal power above a certain frequency while guaranteeing linearity over a specified range. A key benefit is that only an estimate of the first resonance frequency is required during the design. The number of harmonics contained in the scanning signal and the range of linearity can be freely varied to achieve an arbitrarily low out-of-bandwidth power.

The technique is based on finding a signal y that is equal to a reference trajectory r at an arbitrary set of sample indexes S and free to vary elsewhere. The free part of the signal is varied to minimize the quadratic cost $y^T H y$. That is, we seek y that is the solution to

$$y = \arg\min_x x^T H x, \quad \text{subject to } x_k = r_k \quad k \in S, \tag{3}$$

where $x \in \Re^{N\times 1}$ and $H \in \Re^{N\times N}$. Equation (3) is equivalent to the linearly constrained convex quadratic optimization problem

$$y = \arg\min_x x^T H x + 2 f^T x, \quad \text{subject to } Ax = r(S), \tag{4}$$

where A is the selection matrix representing S and $r(S)$ is a row vector containing the samples of r_n indexed by the values of S.

The signal (4) can be restated in matrix notation as

$$\begin{bmatrix} H & A^T \\ A & 0 \end{bmatrix} \begin{bmatrix} y \\ \lambda \end{bmatrix} = \begin{bmatrix} -f \\ r(S) \end{bmatrix}, \tag{5}$$

where λ are the Lagrange multipliers. Equation (5) has a solution

$$\begin{bmatrix} y \\ \lambda \end{bmatrix} = \begin{bmatrix} H & A^T \\ A & \mathbf{0} \end{bmatrix}^{-1} \begin{bmatrix} -f \\ r(S) \end{bmatrix}. \tag{6}$$

It can be shown that minimum out-of-bandwidth power is achieved when [16]

$$H = \frac{1}{N^2} E^* W E, \tag{7}$$

where N is the number of samples per period, E is a fast Fourier transform matrix, and W is a weighting matrix defining which harmonics are penalized and which are to remain free. We apply this technique to determine an input for high-speed scanning.

With a first resonance frequency of 45 kHz (see Fig. 4), the scanner's useful bandwidth is 35 kHz where phase and amplitude deviation is negligible. With a scanning signal containing 7 harmonics (the 1^{st}, 3^{rd}, 5^{th} and 7^{th}), the maximum scan speed is 5 kHz. This corresponds to 25 frames/s at 200×200 resolution, or 50 frames/ second at 100×100 resolution.

A 5 kHz scanning trajectory was designed using the tools described in reference [16][1]. The signal contains 7 significant harmonics and has a linear range of 60%, which equates to a maximum linear scan-range of 7 μm out of a possible 10 μm. The optimal input to achieve the 6 μm trajectory is plotted in Fig. 5(a) together with the industry standard minimum-acceleration signal. The minimum-acceleration signal has the same linear range but follows a quadratic trajectory during the reverse in direction.

In the simulated x-axis displacement plotted in Fig. 5(b), the performance of the optimal signal is clearly demonstrated. The simulation model was obtained by fitting a state-space model to the data of Fig. 4 using the frequency domain subspace algorithm. This technique provides excellent reduced order models over a certain bandwidth. The modal damping ratios were conservatively estimated at 0.005.

The force acting between the sample-mass and actuator can be computed from the numerical acceleration and sample mass using Newton's law. For the trajectory plotted in Fig. 5(b), the maximum tensile force is 10 N per gram of sample. For a maximum load of 2 g and a safety factor of 2, the required preload force is 40 N.

A key scanner performance criteria that strongly influences image quality is the magnitude of runout in adjacent axes. In Fig. 5(c), the y- and z-axis runout resulting from the x-axis trajectory in Fig. 5(b) is plotted. The y-axis runout is less than 0.5% while the z-axis runout is approximately 0.03%. This magnitude of runout is capable of providing 200×200 resolution with negligible image overlap.

V. Electrical Considerations

Due to the capacitive nature of piezoelectric transducers, high speed operation requires large current and power dissipation requirements. If the maximum driving voltage, trajectory, and frequency are known, the current and power dissipation are easily computed by conservatively approximating the transducer as a purely capacitive load.

The current I_p is equal to CsV_p, where C and V_p are the transducer capacitance (380 nF) and load voltage. The power dissipation in a linear amplifier is $P_d = I_p(V_s - V_p)$, where V_s is the supply voltage (200 V). The current, voltage and power dissipation corresponding to the input trajectory in Fig. 5(b) are plotted in Fig. 6. As the load is primarily reactive, the average power dissipation of 75 W is also the required supply power. These specifications can be achieved with standard amplifier configurations.

[1]Available from the second author.

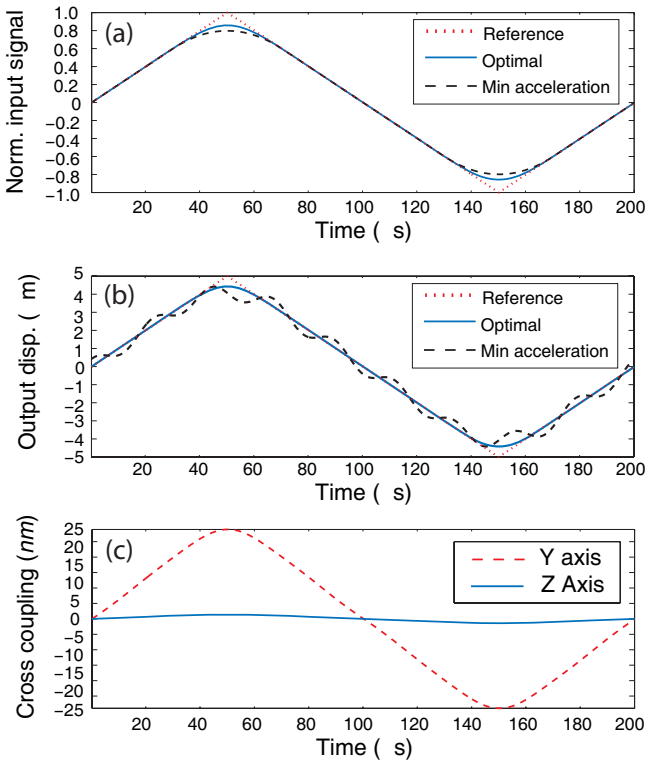

Fig. 5. (a) The scanner input signals: triangular, optimal, and minimum acceleration. (b) The simulated scanner displacement for the optimal and minimum acceleration input. (c) The y- and z-axis runout due to the x-axis trajectory shown in (b).

VI. Preliminary Experimental Results

The manufactured scanner was tested and preliminary results are shown in Fig. 7. A Polytec PSV300 laser vibrometer was used to measure the x- and y-axis displacements. The frequency response plots for the slow and fast scanning directions are shown in Figs. 7(a) and (b), respectively. In the y direction, the first major resonance (piston mode) occurred at approximately 1.5 kHz. This value agrees with the FEA simulation shown in Fig. 4(a2). In the x direction, the first major resonance occurred at approximately 29 kHz. A 100-Hz triangle input voltage [Fig. 7(c)] was applied to drive the high-speed stage. The measured open-loop displacement is shown in Fig. 7(d). Over the range of 9.3 μm, the measured maximum displacement hysteresis was approximately 15%.

VII. Conclusions

This paper describes the design of a two-axis, serial-kinematic high-speed scanner based on piezo-stack actuators. The scanner was designed with a range of 10×10 μm and optimized for high resonance frequency in the fast axis. Experimental results show a good correlation with simulation and a first resonance frequency of 29 kHz was measured in the high-speed axis. This is sufficient to achieve SPM line rates of approximately 4 kHz.

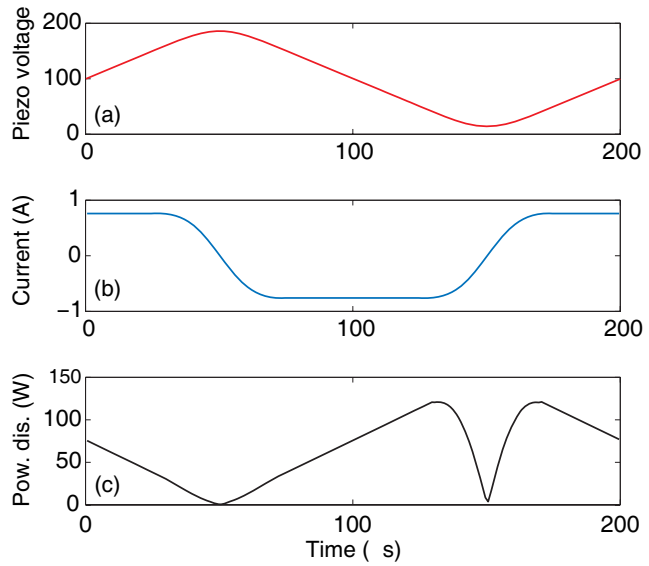

Fig. 6. The (a) voltage, (b) current, and (c) amplifier dissipation required to achieve the trajectory plotted in Fig. 5(b).

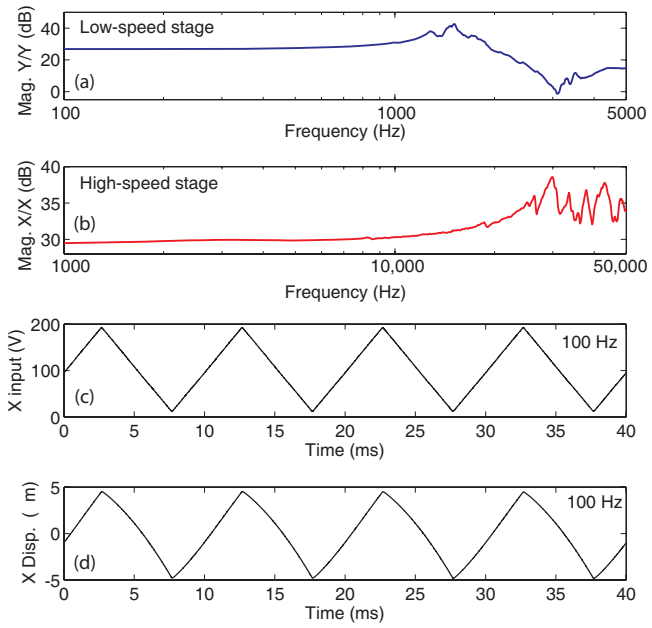

Fig. 7. The measured frequency response of the (a) low- and (b) high-speed stage (units in nm/V). The open-loop (c) input voltage and (d) measured displacement versus time for scanning in the x direction at 100 Hz.

VIII. Acknowledgements

This research was supported, in part, by the National Science Foundation, Grants DUE #0633098 and CMMI #0726778, the Australian Research Council (DP0666620) and the ARC Centre of Excellence for Complex Dynamic Systems and Control. Experiments were performed at the Laboratory for Dynamics and Control of Nanosystems, University of Newcastle. The authors would like to thank Ken Sayce from the University of Newcastle, David Modlin from 3D Enterprises, and Matthew Vaerewyck and Joseph Garthaffner from Virginia Commonwealth University, Richmond, VA, for their help in fabricating the scanner.

References

[1] M. Guthold, X. Zhu, C. Rivetti, G. Yang, N. H. Thomson, S. Kasas, H. G. Hansma, B. Smith, P. K. Hansma, and C. Bustamante. Real-time imaging of one-dimensional diffusion and transcription by Escherichia coli RNA polymerase. *Biophys. J.*, 77(4):2284 – 2294, 1999.

[2] E. S. Snow, P. M. Campbell, and F. K. Perkins. Nanofabrication with proximal probes. *Proc. of the IEEE*, 85(4):601–611, 1997.

[3] T. Ando, N. Kodera, D. Maruyama, E. Takai, K. Saito, and A. Toda. A high-speed atomic force microscope for studying biological macromolecules in action. *Jpn. J. Appl. Phys. Part 1*, 41(7B):4851 – 4856, 2002.

[4] T. Ando, N. Kodera, T. Uchihashi, A. Miyagi, R. Nakakita H. Yamashita, and K. Matada. High-speed atomic force microscopy for capturing dynamic behavior of protein molecules at work. *e-J. Surf. Sci. Nanotech.*, 3:384 – 392, 2005.

[5] G. Schitter, K. J. Astrom, B. E. DeMartini, P. J. Thurner, K. L. Turner, and P. K. Hansma. Design and modeling of a high-speed AFM-scanner. *IEEE Control Systems Technology*, 15(5):906 – 915, 2007.

[6] J. H. Kindt, G. E. Fantner, and J. A. Cutroni P. K. Hansma. Rigid design of fast scanning probe microscopes using finite element analysis. *Ultramicroscopy*, 100(3-4):259 – 265, 2004.

[7] M. J. Rost, L. Crama, P. Schakel, E. van Tol, G. B. E. M. van Velzen-Williams, C. F. Overgauw, H. ter Horst, H. Dekker, B. Okhuijsen, M. Seynen, A. Vijftigschild, P. Han, A. J. Katan, K. Schoots, R. Schumm, W. van Loo, T. H. Oosterkamp, and J. W. M. Frenken. Scanning probe microscopes go video rate and beyond. *Rev. Sci. Instr.*, 76:053710–1 – 053710–9, 2005.

[8] A. D. L. Humphris, J. K. Hobbs, and M. J. Miles. Ultrahigh-speed scanning near-field optical microscopy capable of over 100 frames per second. *Applied Physics Letters*, 83(1):6 – 8, 2003.

[9] G. Schitter. Advanced mechanical design and control methods for atomic force microscopy in real-time. In *American Control Conference*, pages 3503 – 3508, New York City, USA, 2007.

[10] S.O. R. Moheimani and A. J. Fleming. *Piezoelectric transducers for vibration control and damping (advances in industrial control)*. Springer, 2006.

[11] G. Binnig and C. F. Quate. Atomic force microscope. *Phys. Rev. Lett.*, 56(9):930–933, 1986.

[12] W. D. Callister. *Materials science and engineering: an introduction*. John Wiley and Sons, Inc., New York, 1994.

[13] J. Case, L. Chilver, and C. T. F. Ross. *Strength of materials and structures*. John Wiley and Sons, New York, USA, 4th edition, 1999.

[14] D. Croft, G. Shed, and S. Devasia. Creep, hysteresis, and vibration compensation for piezoactuators: atomic force microscopy application. *ASME J. Dyn. Syst., Meas., and Control*, 123:35–43, 2001.

[15] William E. Singhose, Arun K. Banergee, and Warren P. Seering. Slewing flexible spacecraft with deflection-limiting input shaping. *AIAA J. Guidance, Control, and Dynamics*, 20(2):291–298, 1997.

[16] A. J. Fleming and A. Wills. Optimal input signals for bandlimited scanning systems. In *17th IFAC World Congress*, Seoul, Korea, 2008.